Received: 15 April 2019 | Revised: 23 June 2019 | Accepted: 28 June 2019

DOI: 10.1002/aoc.5128

FULL PAPER

WILEY Applied Organometallic Chemistry

Heteroleptic transition metal complexes of Schiff-base-derived ligands exert their antifungal activity by disrupting membrane integrity

Ovas Ahmad Dar[1] | Shabir Ahmad Lone[2] | Manzoor Ahmad Malik[1] | Mohmmad Younus Wani[3] | Md Ikbal Ahmed Talukdar[1] | Abdullah Saad Al-Bogami[3] | Athar Adil Hashmi[1] | Aijaz Ahmad[2,4]

[1] Department of Chemistry, Jamia Millia Islamia, New Delhi 110025, India

[2] Clinical Microbiology and Infectious Diseases, School of Pathology, Faculty of Health Sciences, University of the Witwatersrand, Johannesburg 2193, South Africa

[3] Chemistry Department, Faculty of Science, University of Jeddah, Jeddah, Kingdom of Saudi Arabia

[4] Infection Control, Charlotte Maxeke Johannesburg Academic Hospital, National Health Laboratory Service, Johannesburg 2193, South Africa

Correspondence
Mohmmad Younus Wani, Chemistry Department, Faculty of Science, University of Jeddah, P.O. Box 80327, Jeddah 21589, Kingdom of Saudi Arabia.
Email: mwani@uj.edu.sa

Athar Adil Hashmi, Professor, Department of Chemistry, Jamia Millia Islamia (Central University). New Delhi-110025, India.
Email: aah_ch@yahoo.co.in

Aijaz Ahmad, Senior Medical Scientist, Clinical Microbiology & Infectious Diseases, University of the Witwatersrand. Johannesburg, 2193, South Africa.
Email: aijaz.ahmad@wits.ac.za

Funding information
University Research Committee Grant for 2019 - Friedel Sellschop Award, Grant/Award Number: AZMD019

Development of new treatment strategies and chemotherapeutic agents is urgently needed to combat the growing multidrug resistant species of *Candida*. In this direction, a new series of Cu (II), Co (II), Ni (II) and Zn (II) heteroleptic complexes were synthesized, characterized and evaluated for antifungal activity. Based on spectral characterization and physical measurements, an octahedral geometry was assigned to $[Co(L1)(L2)ClH_2O]$ (**C2**), $[Ni(L1)(L2)ClH_2O]$ (**C3**), $[Zn(L1)(L2)ClH_2O]$ (**C4**) complexes, while a distorted octahedral geometry was assigned to $[Cu(L1)(L2)ClH_2O]$ (**C1**) complex. All the synthesized compounds were tested for antifungal activity against 11 *Candida albicans* isolates, including fluconazole (FLC)-resistant isolates, by determining minimum inhibitory concentrations (MIC) and minimum fungicidal concentrations (MFC), following CLSI guidelines. The mechanism of their antifungal activity was assessed by studying their effect on the plasma membrane using flow cytometry and quantifying the ergosterol contents. All the test compounds showed varying levels of antifungal activity. Both the ligands showed moderate antifungal activity with a median MIC value of 100 μg/mL with no fungicidal activity. Compound **C3** was the most potent compound with median MIC and MFC values of 0.10 and 1.60 μg/mL, respectively. Flow cytometry analysis revealed that these compounds at MFC values disrupt the cell membrane, resulting in propidium iodide entering the cells. These compounds also reduced a considerable amount of ergosterol content after treating the cells with MIC and sub-MIC values. This study indicates that these compounds have high antifungal activity against *C. albicans*, and have the potential to be developed as novel antifungal drugs.

KEYWORDS
Candida albicans, ergosterol, heteroleptic complexes, membrane disruption

1 | INTRODUCTION

The growing incidences of life-threatening systematic fungal infections due to a rise in immunocompromised patient populations and the limited availability of antifungal medications necessitates the development of new antifungal drugs or treatment strategies.[1,2] Fungal diseases, which include pulmonary aspergillosis, cryptococcal meningitis, pneumocystis pneumonia, invasive candidiasis, invasive aspergillosis, disseminated histoplasmosis, fungal asthma and fungal keratitis, kill more than 1.5 million and affect over a billion people worldwide.[3,4] Different antifungal drugs belonging to either azoles or polyenes are currently being used to treat fungal infections, but emergence of drug resistance and treatment failures is a big challenge.[5–7] Among the various strategies to tackle this challenge and curb growing drug resistance and fungal infections, development of new drugs based on a different mechanism of action or drugs that target multiple pathways to evade drug resistance are currently being pursued.[8–10] Complexation of potentially bioactive organic molecules with metals results in a sharp increase in their biological activity. A metal complex usually results in enhanced efficacy compared with the ligand or the metal ion alone, by sometimes the ligands protecting or stabilizing the otherwise reactive metal ion or the metal undergoing redox events that enhance the overall efficacy of the complex, and sometimes the metal and the ligand are mutually responsible for the biological activity of the complex.[11] Coordination compounds offer many binding modes to polynucleotides, including outer-sphere non-covalent binding, metal coordination to nucleobase and phosphate backbone sites, as well as strand cleavage induced by oxidation using redox-active metal centers.[12] The accessibility of different oxidation states of metals such as Fe, Cu, Co, Ru, Mn, etc. may allow for redox chemistry resulting in strand breakage and other alterations, which result in the selective inhibition of the target cell or pathogen.[13]

A diverse range of ligands with different coordination sites have been synthesized and used as chelators for various metal ions. An important class of molecules is the Schiff base ligands; they show great chelating properties due to their azomethine and other coordinating sites or groups. They are stabile under various oxidative and reductive conditions, which make them ideal candidates for the development of new metal-based antimicrobial and anticancer agents.[14–16]

Keeping in view the imperative influence of Schiff bases in medicinal chemistry,[17] and the impact of metallodrugs as potential chemotherapeutic agents, our main rationale of this study was to explore whether the incorporation of a transition metal ion, a Schiff base derived from biologically important scaffolds in the form of heteroleptic complexes, would deliver a synergistic effect and thus act as a hopeful stratagem for development of effective chemotherapeutic agents. Literature reveals that the Schiff base ligands derived from 1,4-benzodioxane-6-amine have not been much studied, and the Schiff bases derived from 4-(dimethyl-amino)benzaldehyde show great pharmacological effects.[18–21] Therefore, in the present study some new heteroleptic complexes derived from two different bidentate Schiff base ligands have been synthesized, and their promising antifungal potential was evaluated against different fluconazole (FLC)-susceptible and -resistant *Candida albicans* isolates in a quest to find a better antifungal agent.

2 | EXPERIMENTAL

2.1 | Materials and physical methods

All the chemicals used were of reagent grade, and were used without further purification. 1,4-Benzodioxane-6-amine and 2-hydroxy-1-naphthaldehyde were purchased from Sigma-Aldrich Chemie (Germany). Ethylenediamine, metal chlorides and ethanol were purchased from Merck. 4-(dimethyl-amino)Benzaldehyde was purchased from Sd-fine.

The prepared Schiff base ligands and metal complexes were subjected to microanalyses (C, H and N) that were carried out with Elementar (Thermo Scientific). The molar conductivities of freshly prepared solutions at room temperature were measured on a Syntronics type 302 conductivity bridge equilibrated at 25 ± 0.01°C. For conductivity measurements, 1 mM solutions in dimethylsulfoxide (DMSO) were prepared. Electrothermal melting point apparatus was used to determine the melting point of the synthesized compounds. UV–Vis spectra were recorded between 200 and 800 nm using UV–Vis spectrophotometer (UV-260 Shimadzu, with 1-cm quartz cuvettes). Fourier transform-infrared (FT-IR) spectra of the Schiff base ligands and metal complexes were investigated using KBr pellets on a Perkin-Elmer 283 spectrophotometer. ^{1}H-NMR and ^{13}C-NMR measurements were recorded using Brucker WH 300 (200 MHz) and Brucker WH 270 (67.93 MHz) using DMSO-d_6 as a solvent and tetramethylsilane as an internal standard. ESI-MS (AB-Sciex 2000, Applied Biosystem) was used to record mass spectra of the synthesized ligands and complexes. The magnetic susceptibility of the investigated compounds was measured using the Faraday balance. Powder X-ray diffraction (XRD) studies of the synthesized compounds were carried out at room temperature using Rigaku, Mini Flex II powder diffractometer using CuKα

monochromatic radiation (λ = 1.5406 Å) in the range of $10° \leq 2\theta \leq 80°$. The thermogravimetric analysis (TGA/DTG) was carried out in the temperature range of 20–1000°C in a dynamic nitrogen atmosphere with a heating rate of 10°C/min using NETZSCH STA 449F3 thermal analyzer.

2.2 | Synthesis

2.2.1 | Synthesis of Schiff base ligand (L1)

The Schiff base ligand *N*,*N*′-bis(4-dimethylamino) benzylidene-ethane-1,2-diamine (**L1**) was synthesized by the condensation reaction of 4-(dimethyl-amino)benzaldehyde (0.60 g, 4 mmol) and ethylenediamine (0.13 ml, 2 mmol) dissolved in ethanol in the stoichiometric ratio of 2:1, respectively, and the reaction mixture was stirred in a round-bottom flask for 4 hr at room temperature (approximately 25°C). The reaction was monitored by taking thin-layer chromatography at regular intervals. The white precipitate obtained was separated by filtration, washed with water and diethyl ether, and dried in vacuum over $CaCl_2$ for further use. Synthetic outline of the Schiff base ligand is shown in Scheme 1.

Color: off white; yield: 82%. Elemental anal. calcd for $C_{20}H_{26}N_4$: C, 74.50; H, 8.13; N, 17.38; found: C, 73.77; H, 8.10; N, 17.40; IR (KBr pellet, cm^{-1}): 1590 υ(-HC=N-), 1344 $\upsilon(C\text{-}N)_{aromatic}$, 1162 $\upsilon(C\text{-}N)_{aliphatic}$, 1480 υ(C=C), 2915υ(-$CH_2$-). ^{1}H-NMR (DMSO-$d_6$, δ, ppm): 8.65 (s, 2H, CH=N), 3.05 (s, 12H, N-$(CH_3)_4$), 3.73 (s, 4H, N-CH_2), 6.69–7.52 (m, 8H, ArH). ^{13}C-NMR (DMSO-d_6, δ, ppm): 161.70 (-HC=N-), 40.60 (-CH_3), 61.86 (-CH_2-), 111.94, 124.50, 129.54, 152.23 (-C_6H_4-). Mass spectrum (ESI) $[M + H]^+$ = 323.2. UV–Vis (DMSO): λ/nm 286, 328.

2.2.2 | Synthesis of Schiff base ligand (L2)

(*E*)-1-(((2,3-dihydrobenzo[1,4]dioxin-6-yl)imino)methyl) Naphthalen-2-ol (**L2**) was synthesized from the condensation of 2-hydroxy-1-naphthaldehyde (0.86 g, 5 mmol) and 1,4-benzodioxane-6-amine (0.75 g, 5 mmol) dissolved in ethanol in the molar ratio of 1:1, respectively. The reaction mixture was stirred at room temperature for 4 hr. The yellow precipitate formed was filtered, and washed thoroughly with the least amount of ethanol and diethyl ether. Finally, the residue was collected and dried in a desiccator over anhydrous calcium chloride for further use.

Color: yellow; yield: 78%. Elemental anal. calcd for $C_{19}H_{15}NO_3$: C, 74.72; H, 4.95; N; 4.59; found: C, 74.80; H, 5.05; N, 4.62. IR (KBr pellet, cm^{-1}): 1610 υ(-CH=N-), 3251 υ(OH), 1286 υ(C-O), 1257 υ(C-O-C). ^{1}H-NMR (DMSO-d_6, δ, ppm): 9.59 (s, 1H, CH=N), 4.29(s, 4H, -OCH_2), 13.15 (s, 1H, OH), 6.94–8.51 (m, 9H, ArH).^{13}C-NMR (DMSO-d_6, δ, ppm): 170.05 (C-OH), 155.80 (CH=N), 144.96 (C-N),143.38 (C-O), 65.05–65.09 (-OCH_2), 109.46–138.73 (Ar Cs). Mass spectrum (ESI) $[M + Na]^+$ = 328.09. UV–Vis (DMSO): λ/nm 272, 330.

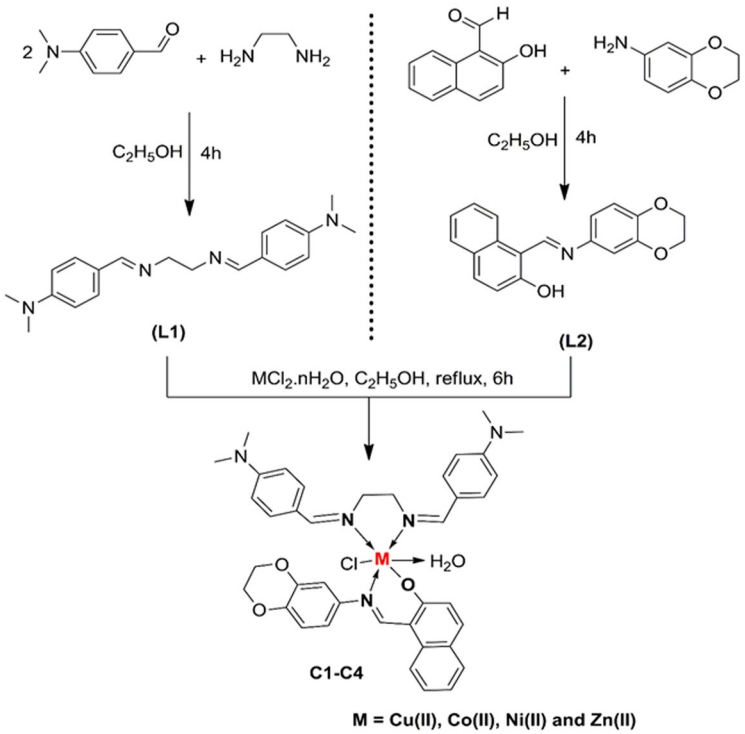

SCHEME 1 Synthesis of Schiff base ligands (**L1** and **L2**) and their heteroleptic complexes (**C1–C4**)

2.2.3 | Synthesis of heteroleptic metal complexes (C1–C4)

Ethanolic solution (15 ml) of metal salts, $[M(Cl_2)\cdot nH_2O]$ (2 mmol) was added to hot ethanolic solution (20 ml) of Schiff base ligand (**L1**) with constant stirring, and then after a few minutes an ethanolic solution of Schiff base ligand (**L2**) was added. Triethylamine was added to maintain the pH of solution. The reaction mixture was then refluxed for about 5–6 hr at 80°C. The reaction mixture was then cooled to room temperature. The precipitate formed was filtered, washed thoroughly with ethanol followed by diethyl ether to remove the unreacted compounds, and finally dried in a vacuum over fused calcium chloride in a desiccator.

[Cu(L1)(L2)Cl·H_2O] (C1)
Color: pale green; yield: 68%. Elemental anal. calcd for $[C_{39}H_{42}ClCuN_5O_4]$: C, 62.98; H, 5.69; N, 9.42; found: C, 63.72; H, 5.72; N, 9.47. IR (KBr pellet, cm^{-1}): 1585 υ(CH=N), 1298 $\upsilon(C\text{-}O_{phenol})$, 1359 $\upsilon(C\text{-}N)_{aromatic}$, 1178 $\upsilon(C\text{-}N)_{aliphatic}$, 1263 υ(C-O-C), 3490 υ OH), 562 υ(Cu-O), 448 υ(Cu-N). Mass spectrum (ESI) $[M + H]^+ = 742.3$.

[Co(L1)(L2)Cl·H_2O] (C2)
Color: black; yield: 65%. Elemental anal. calcd for $[C_{39}H_{42}ClCoN_5O_4]$: C, 63.37; H, 5.73; N, 9.47; found: C, 63.40; H, 5.79; N, 9.52. IR (KBr pellet, cm^{-1}): 1592 υ(CH=N), 1350 $\upsilon(C\text{-}N)_{aromatic,}$ 1290 $\upsilon(C\text{-}O_{phenol})$, 1263 υ(C-O-C), 1166 $\upsilon(C\text{-}N)_{aliphatic}$, 3497 υ(OH), 562 υ(Co-O), 457 υ(Co-N). Mass spectrum (ESI) $[M + H]^+ = 739.3$.

[Ni(L1)(L2)Cl·H_2O] (C3)
Color: brown; yield: 69%. Elemental anal. calcd for $[C_{39}H_{42}ClN_5NiO_4]$: C, 63.39; H, 5.73; N, 9.48; found: C, 63.09; H, 5.76; N, 9.57. IR (KBr pellet, cm^{-1}): 1582 υ(CH=N), 1290 $\upsilon(C\text{-}O_{phenol})$, 1347 $\upsilon(C\text{-}N)_{aromatic}$, 1165 $\upsilon(C\text{-}N)_{aliphatic}$, 1262 υ(C-O-C), 3495 υ(OH), 556 υ(Ni-O), 460 υ(Ni-N). Mass spectrum (ESI) $[M + H]^+ = 738.8$.

[Zn(L1)(L2)Cl·H_2O] (C4)
Color: orange yellow; yield: 70%. Elemental anal. calcd for $[C_{39}H_{42}ClN_5O_4Zn]$: C, 62.82; H, 5.68; N, 9.39; found: C, 63.12; H, 5.72; N, 9.60. IR (KBr pellet, cm^{-1}): 1590 υ(CH=N), 1302 $\upsilon(C\text{-}O_{phenol})$, 1353 $\upsilon(C\text{-}N)_{aromatic}$, 1175 $\upsilon(C\text{-}N)_{aliphatic}$, 1264 υ(C-O-C), 3497 υ(OH), 570 υ(Zn-O), 475 υ(Zn-N). ^{1}H-NMR (DMSO-d_6, δ, ppm): 8.72, (s, 2H, CH=N), 9.60 (s, 1H, CH=N), 3.14 (s, 12H, N-$(CH_3)_4$), 3.80 (s, 4H, N-CH_2),4.37 (s, 4H, -OCH_2), 6.69–7.89 (m, ArH). ^{13}C-NMR (DMSO-d_6, δ, ppm): 162.30, 156.85 (-HC=N-), 42.65 (-CH_3), 61.19 (-CH_2-), 170.15 (C-O), 145.51 (C-N), 143.44 (-O-C), 65.10 (-OCH_2), 109.47–138.57 (Ar Cs). Mass spectrum (ESI) $[M + H]^+ = 743.7$.

3 | BIOLOGICAL INVESTIGATIONS

3.1 | Strains, media and chemicals

All the strains used in this study are detailed in Table 3, which consists of eight FLC-susceptible (including one laboratory strain *C. albicans* SC5314 and seven clinical isolates) and three FLC-resistant clinical isolates. All the clinical *C. albicans* strains were collected from Charlotte Maxeke Johannesburg Academic Hospital, Johannesburg, South Africa, and were stored in glycerol stocks at−80°C in the Department of Clinical Microbiology and Infectious Diseases. All the test strains were isolated from patients under the ethical clearance number M10102 obtained from the Human Research Ethics Committee, University of the Witwatersrand. Prior to experiments, *Candida* isolates were revived by plating on Sabouraud Dextrose (SD) Agar (Sigma Aldrich, USA), followed by growing single colonies in fresh SD broth. FLC and amphotericin were purchased from Sigma Fluke (USA). All other chemicals and media were purchased from Sigma Aldrich and Merck.

TABLE 1 Physico-chemical properties of Schiff base ligands (**L1** and **L2**) and their heteroleptic complexes (**C1–C4**)

Compound	Color	Mol. formula	Mol. wt.	(m/z) ratio	Yield (%)	Λ_m (Ω^{-1} cm^2 mol^{-1})	m.p. (°C)	μ_{eff} (B.M.)
L1	Off white	$C_{20}H_{26}N_4$	322.4	323.2	82	–	190	–
L2	Yellow	$C_{19}H_{15}NO_3$	305.3	328.0	78	–	192	–
C1	Pale green	$[C_{39}H_{42}ClCuN_5O_4]$	742.2	742.3	68	26	252	1.90
C2	Black	$[C_{39}H_{42}ClCoN_5O_4]$	738.2	739.3	65	20	285	4.90
C3	Brown	$[C_{39}H_{42}ClN_5NiO_4]$	737.2	738.8	69	17	310	3.70
C4	Orange Yellow	$[C_{39}H_{42}ClN_5O_4Zn]$	743.2	743.7	70	22	290	Diamag.

TABLE 2 Thermoanalytical results (TG and DTG) of heteroleptic complexes (**C1–C4**)

Complex	TG range (°C)	DTG_{max} (°C)	*n**	Found (calcd %) Weight loss	Total weight loss	Assignment	Metallic residue
$[C_{39}H_{42}ClCu\ N_5O_4]$	100–230	148,222	2	6 (7.18)		Loss of one coordinated H_2O and $\frac{1}{2}Cl_2$ molecule	Cu
	230–490	347	1	40 (41.07)	88 (91.62)	Loss of $C_{19}H_{15}NO_3$	
	490–800	660	1	42 (43.37)		Loss of $C_{20}H_{26}N_4$	
$[C_{39}H_{42}ClCoN_5O_4]$	100–220	142,220	2	6.50 (7.24)		Loss of one coordinated H_2O and $\frac{1}{2}Cl_2$ molecule	Co
	220–480	315	1	40.50 (41.33)	89.40 (92.21)	Loss of $C_{19}H_{15}NO_3$	
	480–880	674	1	42.40 (43.64)		Loss of $C_{20}H_{26}N_4$	
$[C_{39}H_{42}ClN_5NiO_4]$	100–240	130,229	2	6 (7.22)		Loss of one coordinated H_2O and $\frac{1}{2}Cl_2$ molecule	Ni
	240–500	376	1	40 (41.37)	89 (92.39)	Loss of $C_{19}H_{15}NO_3$	
	500–920	754	1	43 (43.8)		Loss of $C_{20}H_{26}N_4$	
$[C_{39}H_{42}ClN_5O_4Zn]$	100–250	120,220	2	6 (7.18)		Loss of one coordinated H_2O and $\frac{1}{2}Cl_2$ molecule	Zn
	250–540	287	1	41 (41.03)	90 (91.56)	Loss of $C_{19}H_{15}NO_3$	
	540–790	710	1	43 (43.35)		Loss of $C_{20}H_{26}N_4$	

*n** = number of decomposition.

TABLE 3 MICs (μg/ml) of ligands (**L1**, **L2**) and the complexes (**C1–C4**) against FLC-susceptible and -resistant *Candida albicans* isolates

Strains		MICs (μg/mL) L1 MIC	L1 MFC	L2 MIC	L2 MFC	C1 MIC	C1 MFC	C2 MIC	C2 MFC	C3 MIC	C3 MFC	C4 MIC	C4 MFC	FLC MIC
	Candida albicans SC5314	100	–	100	–	6.25	12.5	0.40	3.12	0.10	1.60	12.5	25	0.25
FLC-susceptible	4175	100	–	100	–	6.25	12.5	0.40	3.12	0.10	1.60	12.5	25	0.12
	4179	100	–	50	–	12.5	12.5	3.12	6.25	0.20	3.12	50	50	0.25
	4180	100	–	100	–	6.25	12.5	0.40	3.12	0.10	1.60	12.5	25	0.25
	4251	100	–	100	–	6.25	12.5	0.40	3.12	0.10	1.60	12.5	50	0.25
	4554	100	–	50	–	6.25	12.5	0.40	3.12	0.10	1.60	12.5	50	0.25
	4563	100	–	100	–	6.25	12.5	1.60	3.12	0.20	1.60	12.5	25	0.25
	4576	100	–	100	–	6.25	12.5	0.40	3.12	0.10	1.60	12.5	25	0.25
FLC-resistant strains	4085	100	–	100	–	12.5	50	1.60	6.25	0.20	3.12	25	50	16
	4122	100	–	100	–	12.5	50	3.12	6.25	0.40	3.12	50	50	32
	4135	100	–	100	–	12.5	50	1.60	6.25	0.20	3.12	25	50	32

FLC, fluconazole; MIC, minimum inhibitory concentration.

3.2 | Antifungal susceptibility tests

3.2.1 | Determination of minimum inhibitory concentrations and minimum fungicidal concentrations

To determine the antifungal activity of newly synthesized Schiff base ligands (**L1** and **L2**) and their four complexes (**C1–C4**), minimum inhibitory concentrations (MICs) were determined against tested FLC-susceptible and FLC-resistant *C. albicans* isolates by serial micro-broth dilution assay following Clinical and Laboratory Standards Institute (CLSI)-recommended guidelines M27-A3,[22] with modifications. The initial concentrations of all the newly synthesized compounds were 400 μg/mL, in order to achieve the concentrations of 100, 50, 25, 12.5, 6.25, 3.12, 1.60, 0.8, 0.4, 0.2, 0.1 and 0.05 μg/mL in a 96-well plate after serial dilution. The positive control FLC (1000 μg/mL) and the negative vehicle control (1% DMSO) were also included in every set of experiments. Media and culture controls were included to confirm the sterility and viability, respectively. Further, minimum fungicidal concentration (MFC) was determined by subculturing the test dilutions from each well without color change on SD

agar plates and incubated for 24 hr. The lowest concentration that showed no fungal growth on the agar plate was defined as the MFC value. All the experiments were done in triplicate, and all the results were expressed in μg/mL.

3.2.2 | Sterol quantification

To study the effect of newly synthesized compounds on the ergosterol biosynthesis pathway, total intracellular sterols were extracted and quantified using a spectrophotometer, as reported previously.[23] One FLC-susceptible and one -resistant isolate of *C. albicans* cells were treated with MIC and ½ MIC values of both the ligands and their four derivatives. In all the tests, there is a negative control (without test compound) and positive control (2 μg/mL FLC). All the sterol samples were scanned spectrophotometrically between 240 and 300 nm, using a spectrophotometer. The presence of ergosterol and the late sterol intermediate 24(28) DHE in the extracted sample resulted in a characteristic four-peaked curve. The absence of detectable ergosterol in extracts was indicated by a flat line. Ergosterol content was calculated as a percentage of the wet weight of the cell, using the following equations:

$$\%\text{ergosterol} + \%24(28)\ \text{DHE} = [(A_{281.5}/290) \times F]/\text{pellet weight}$$
$$\%24(28)\ \text{DHE} = [(A_{230}/518) \times F]/\text{pellet weight}$$
$$\%\text{ergosterol} = [\%\text{ergosterol} + \%24(28)\ \text{DHE}] - \%24(28)\ \text{DHE}$$

where F is the factor for dilution in ethanol, and 290 and 518 are the E values (in percentages per centimeter) determined for crystalline ergosterol and 24(28) DHE, respectively.

3.2.3 | Effect on membrane permeability

Based on the MIC results, all the active compounds (**C1**, **C2**, **C3** and **C4**) except the ligands were tested to study the effect on membrane integrity, by doing flow cytometry using propidium iodide (PI). PI is a fluorescent dye with a characteristic to enter into necrotic cells with disintegrated membranes. Mid-exponentially grown *C. albicans* cells were exposed to MFC values of the test entities for 2 hr. After the exposure time, cells were harvested and resuspended in phosphate-buffered saline. To this solution, 1 mL of PI was added with a final concentration of 1 mg/mL of PI. All the samples were incubated at 35°C for 15 min in the dark at room temperature. In every set of experiments, negative (untreated cells) and positive (2 μg/mL amphotericin B-treated cells) controls were included. Unstained cells were always included as autofluorescence controls. Cell-associated fluorescence was measured using a flow cytometry BD LSRFortessa cell analyzer (Becton Dickinson, USA). The results were analyzed using FlowJo software version 10.0. For data analysis, quadrants were adjusted, analyzed and interpreted as reported earlier.[24]

4 | RESULTS AND DISCUSSION

The heteroleptic complexes (**C1–C4**) were successfully prepared by reacting equimolar amounts of Schiff base ligands (**L1** and **L2**) with the corresponding metal salts in the presence of triethylamine. The metal complexes were neutral, colored, air-stable, and insoluble in water and common organic solvents but remarkably soluble in DMF and DMSO. Synthesis and the final structures of the ligands and their complexes were verified by different physical and spectroscopic techniques. The different physico-chemical properties of Schiff base ligands (**L1** and **L2**) and metal complexes (**C1–C4**) are shown in Table 1. The molar conductivity (Λm) of the complexes was carried out using DMSO (10^{-3} M) at 25°C. The results obtained were in the range of 17–26 $\Omega^{-1}cm^2m^{-1}$, which showed their non-electrolytic nature.

4.1 | Magnetic susceptibility and electronic spectral studies

The geometry of the synthesized heteroleptic complexes was obtained from the electronic spectral data and magnetic susceptibility measurements. The electronic absorption spectra of the ligands (**L1** and **L2**) and their complexes (**C1–C4**) were recorded in 10^{-3} M DMSO solution in the range of 200–800 nm using the same solvent as blank. The UV–Vis spectrum of **L1** displayed two absorption bands at 286 and 328 nm, and **L2** also showed two absorption bands at 272 and 330 nm corresponding to π-π* and *n*-π* transitions, respectively. In complexes, these bands were shifted towards lower or higher wavelengths signifying the coordination of ligands to metal ions, as shown in Figure 1. The addition of metal ion to ligands produced characteristic changes in the visible absorption spectrum of the ligands, signifying the complex formation. In complexes, a band appeared in the region 352–424 nm corresponding to charge transfer from ligand to metal. In complex **C1** the absorption band appearing at 398 nm can be attributed to charge transfer from ligand to metal. The broad asymmetric band in **C1** appearing at 681 nm corresponded to a combination of three bands $^2B_{1g} \rightarrow {}^2A_{1g}$ (υ_1), $^2B_{1g} \rightarrow {}^2B_{2g}$ (υ_2) and $^2B_{1g} \rightarrow {}^2E_g$ (υ_3), which are similar in energy. The broadness of the band showed its distortion from the octahedral geometry and provided the indication for Jahn Teller distortion.[25,26] The magnetic moment of this

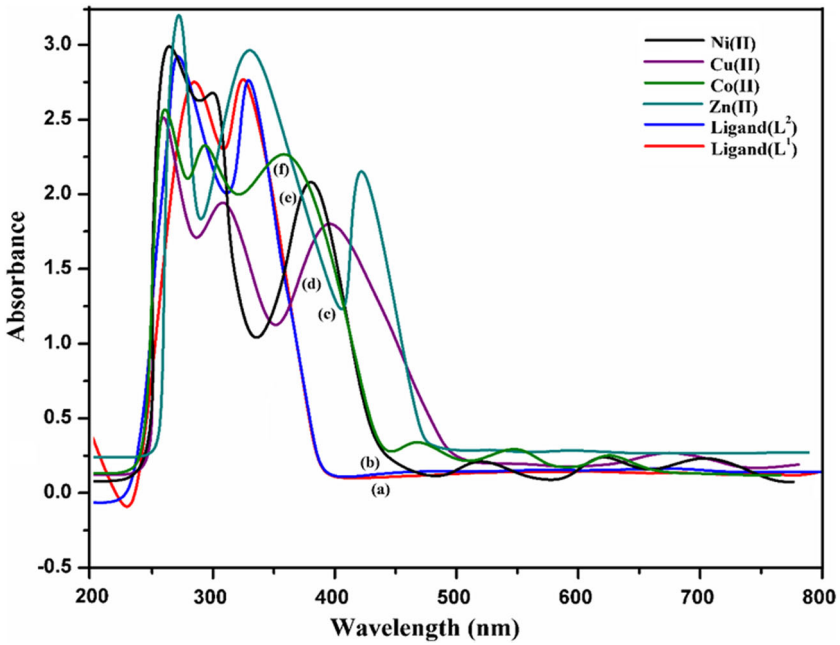

FIGURE 1 UV–Vis spectra of: (a) Schiff base (**L1**); (b) L2; (c) Zn (II); (d) Cu (II); (e) Ni (II); and (f) Co (II) complexes in 10^{-3} M dimethylsulfoxide (DMSO) solution

complex was found to be 1.90 B.M., which lies within the normal range for octahedral Cu (II) complexes. The electronic absorption spectrum of **C2** shows bands at 460, 550 and 630 nm that are assigned to $^4T_{1g}(F) \rightarrow {}^4T_{1g}(P)$, $^4T_{1g}(F) \rightarrow {}^4A_{2g}(F)$ and $^4T_{1g}(F) \rightarrow {}^4T_{2g}(F)$, respectively. The band at 382 nm corresponds to ligand to metal charge transfer band.[27] The magnetic moment of complex (**C2**) was found to be 4.90 B.M. The absorption bands and the magnetic moment suggested an octahedral geometry around the Co (II) ion. The absorption spectrum of **C3** displayed three absorption bands at 521, 634 and 705 nm, which may be attributed to $^3A_{2g} \rightarrow {}^3T_{1g}(P)$, $^3A_{2g} \rightarrow {}^3T_{1g}(F)$ and $^3A_{2g} \rightarrow {}^3T_{2g}$ transitions, respectively.[28] The spectrum also displayed a band at 398 nm, which may be assigned to ligand to metal charge transfer. The magnetic moment observed for complex **C3** was found to be 3.7 B.M. The absorption spectra and magnetic moment reveal that there is an octahedral geometry around the Ni (II) ion. In **C4** the absorption band found at 424 nm may be attributed to the ligand to metal charge transfer with zero magnetic moment. Due to the diamagnetic nature of complex **C4**, no d-d bands were observed. An octahedral geometry has been proposed for the complex **C4**.

4.2 | FT-IR spectra

The IR spectra of the complexes were compared with those of the free Schiff base ligands (**L1** and **L2**) to verify the coordination sites that may be involved in chelation. In complexes, the position or intensity of the peaks obtained for ligands are expected to change upon chelation. The characteristic peaks are given in Section 2.2. The sharp band observed at 1602 cm^{-1} in the spectrum of free Schiff base ligand (**L1**) was assigned to υ (CH=N) stretching vibrations. In Schiff base ligand (**L2**), the υ(CH=N) stretching vibration was found at 1610 cm^{-1}. In the spectra of metal complexes, the υ(CH=N) stretching vibrations of azomethine were shifted to lower wavenumbers, which revealed the participation of the azomethine nitrogen in coordination. The participation of deprotonated phenolic OH in complexation was verified by the blue shift of υ(C-O) stretching band, present at 1286 cm^{-1} in the free ligand **L2**, which shifted to higher wavenumbers by 4–16 cm^{-1} in complexes. The IR spectrum of the **L2** ligand displayed a broad band at 3152 cm^{-1}, which could be assigned to the phenolic OH group.

In complexes (**C1–C4**), the broad bands present at 3490–3497 cm^{-1} might be attributed to the stretching frequencies of the υ(OH) of coordinated water molecules present in these complexes. In Schiff base ligand **L2** and complexes, the bands present at 1256–1263 cm^{-1} were assigned to C-O-C stretching vibrations. In complexes **C1–C4**, new bands are found in the regions 556–570 cm^{-1}, which were attributed to υ(M-O) stretching vibrations, and the bands present at 448–475 cm^{-1} in complexes have been ascribed to υ(M-N) of the azomethine mode. Therefore, from the IR spectra data it was revealed that the ligand (**L1**) behaves as a bidentate ligand with NN donor sites coordinating to the metal ions through

azomethine N atoms. The ligand (**L2**) also behaves as a bidentate ligand with NO donor sites coordinating to metal ions through azomethine N and phenolic O atoms. The IR spectra of the Schiff base ligands (**L1** and **L2**) and complex **C3** as an example is shown in Figure 2, and the spectra of complexes (**C1**, **C2** and **C4**) are given in the supplementary data.

4.3 | ^{1}H-NMR and ^{13}C-NMR spectra

The ^{1}H-NMR spectral data of the Schiff base ligands (**L1**, **L2**) and **C4** complex were recorded in DMSO-d_6 for the interpretation of number and nature of protons relative to TMS with chemical shifts given in ppm. The ^{1}H-NMR spectra of the Schiff bases (**L1** and **L2**) displayed singlet signals at 8.65 and 9.59 ppm, respectively, attributed to the protons of azomethine nitrogen (CH=N), which confirmed the formation of Schiff base ligands. In **C4** complex, a shift of electron density from ligands to metal ion has been detected. The signal for the azomethine protons is slightly deshielded and appeared at 8.72 and 9.60 ppm, and this downfield shift confirms the coordination of azomethine nitrogen with the Zn (II) metal ion (Figure 3). In **L1**, the two sharp singlets at 3.73 and 3.05 ppm are ascribed to active methylene protons (-CH_2 and -N-$(CH_3)_4$), respectively. The ^{1}H-NMR spectra of **L2** exhibited a sharp singlet at 4.29 ppm attributed to methylene protons (-OCH_2). The Ph-OH proton of **L2** appeared as a singlet at 13.15 ppm.[29] In **C4** complex, the Ph-OH proton signal was found absent confirming the complexation through phenolic oxygen. In **C4** complex, a new signal has been found at 3.48 ppm due to the presence of coordinated H_2O protons. The aromatic protons in **C4** complex appeared as a set of multiplets in the region of 6.69–7.89 ppm. The positions of the main signals in the ^{1}H-NMR and ^{13}C-NMR are stated in the Experimental section. The attained ^{13}C values of **C4** complex were compared with the corresponding ligands and were in good agreement with the proposed structure of the **C4** complex. In Schiff base ligands (**L1** and **L2**), the azomethine carbon atoms were observed at 161.70 and 155.80 ppm, which were shifted to 162.30 and 156.85 ppm in **C4** complex, respectively. The paramagnetic **C1**, **C2** and **C3** complexes did not show fine NMR spectra and were therefore not included in this study. The ^{1}H-NMR of Schiff base ligands and ^{13}C-NMR of **L1**, **L2** and **C4** are shown in the supplementary data.

4.4 | Mass spectra

The mass spectra of the Schiff base ligands (**L1**, **L2**) and complexes (**C1–C4**) are characterized by moderate to high

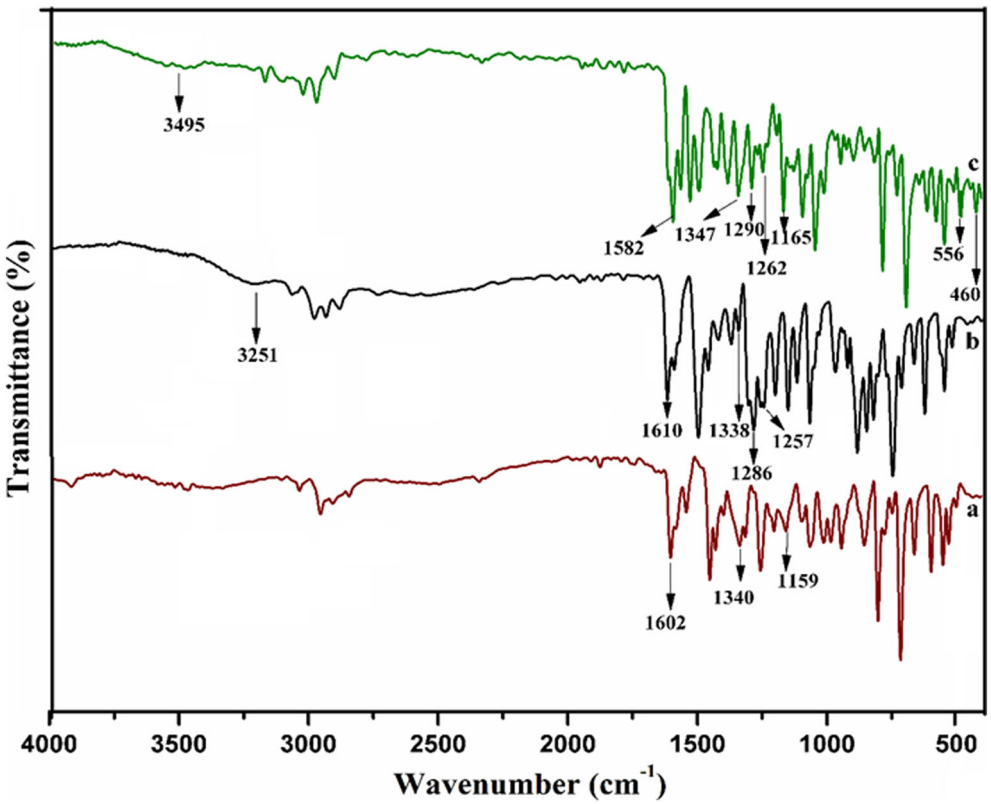

FIGURE 2 Fourier transform-infrared (FT-IR) spectra of: (a) Schiff base (**L1**); (b) Schiff base (**L2**); and (c) Ni (II) complex (**C3**)

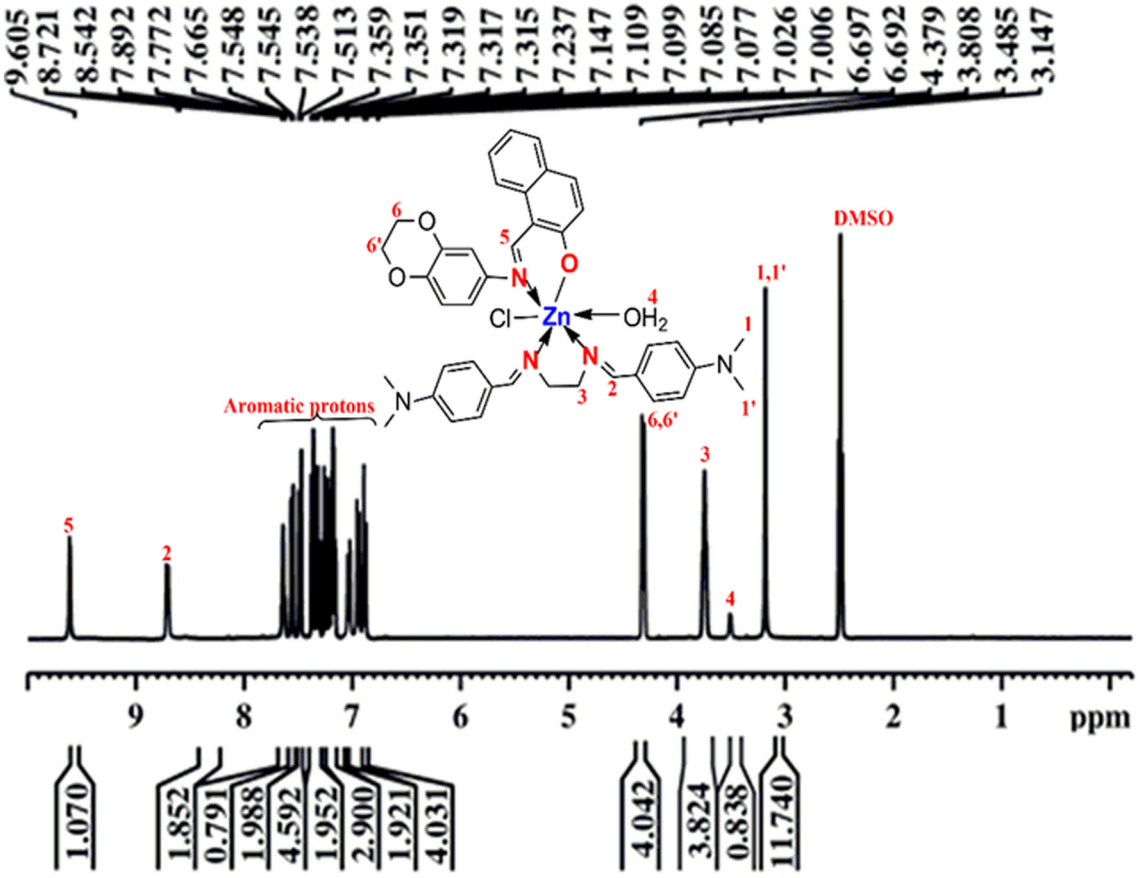

FIGURE 3 ^{1}H-NMR spectrum of **C4** complex in dimethylsulfoxide (DMSO)-d_6

relative intensity molecular ion peaks. It is noticeable that the molecular ion peaks are in good agreement with the suggested empirical formula of the compounds. The mass spectra $[M + H]^+$of Schiff base ligand (**L1**) showed the molecular ion peak at m/z 323.2, and the mass spectra $[M + Na]^+$ of **L2** showed the molecular ion peak at m/z 328.0. The mass spectra $[M + H]^+$ of metal complexes (**C1**, **C2**, **C3** and **C4**) showed molecular ion peaks at 742.3, 739.3, 738.8 and 743.7, respectively. The mass spectra of the synthesized compounds are given in the supplementary data.

4.5 | Powder X-ray diffraction studies

All the efforts failed to grow single crystals of synthesized compounds suitable for single X-ray crystallography. So, X-ray powder diffraction studies of the compounds were carried out to get more details about their structure. The powder XRD of the compounds were carried out in the range 10-80^{o} (θ) at a wavelength of 1.54 Å. The XRD pattern indicates that the ligands (**L1**, **L2**) and complexes (**C1**, **C2**, **C4**) have well-defined crystalline patterns with various degrees of crystallinity. The XRD pattern of **L1**, **L2** and complex **C1** is shown in Figure 4. In complex **C3**, the trend of curves decreases from maximum to minimum intensity indicating its amorphous nature. Some new extra peaks were found in complexes as compared with ligand, signifying the coordination of ligand to metal ions. The XRD of ligand (**L1**) displayed reflecting peaks at 2θ scattering angles of 11.50, 14.30, 17.97, 23.92, 25.73 and 27.10. The **L2** exhibited reflecting peaks at 2θ scattering angles of 15.94, 19.62, 20.64, 23.78, 24.98 and 28.86, while complex **C1** exhibited reflecting peaks at 2θ scattering angles of 15.87, 17.10, 20.10, 20.42, 22.50, 25.10, 26.94 and 29.50 assigned to (100), (110), (111), (021), (111), (121), (102) and (022) crystal planes, respectively, characteristic of well-ordered monoclinic arrangement of Cu atoms (space group: P21/c, JCPDS: 72–0438). The complex **C2** displayed fine reflecting peaks at 2θ scattering angles of 15.03, 15.70, 17.38, 18.70, 23.15, 23.40, 25.70, 31.30 and 33.28 ascribed to (100), (001), (110), (111), (120), (021), (101), (131) and (202) crystal planes, respectively, characteristic of well-ordered monoclinic arrangement of Co atoms (space group: P21/m, JCPDS: 75–2160), whereas complex **C4** showed reflecting peaks at 2θ scattering angles of 11.35, 13.54, 15.12, 19.63, 20.43, 22.12 and 29.85 assigned to (010), (110), (111), (210), (211), (113) and (123) crystal planes, respectively,

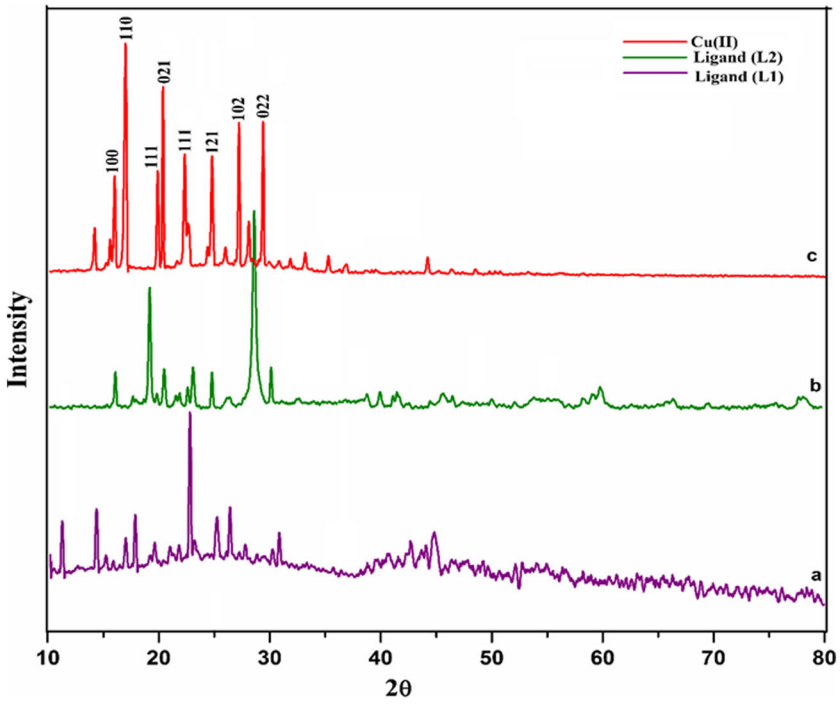

FIGURE 4 Powder X-ray diffraction (XRD) pattern of: (a) Schiff base ligand (**L1**); (b) **L2**; and (c) **C1** complex

characteristic of well-organized orthorhombic arrangement of Zn atoms (space group: $Pca2_1$, JCPDS: 76–0778). The detailed XRD parameters of the complexes are listed in Table S1.

The average crystallite size of the ligands (**L1** and **L2**) and the complexes (**C1**, **C2** and **C4**) was estimated using the Debye Scherrer's formula.[30]

$$D = 0.9\lambda / \beta\cos\theta$$

where constant 0.9 is the shape factor, D is the particle size, λ is the X-ray wavelength of CuKα radiation (1.5406 Å), θ is the Bragg diffraction angle and β is the full-width at half-maximum value of θ.[30] The average crystallite sizes of the ligands (**L1** and **L2**) and the complexes (**C1, C2** and **C4**) were found to be 30.79, 30.18, 39.87, 26.68 and 34.28 nm, respectively.

4.6 | Thermal analysis (TG and DTG)

The thermal analysis of the complexes (**C1–C4**) was studied by using thermogravimetric techniques (Thermal Gravimetric Analysis and Derivative Thermogravimetry) within a temperature range from room temperature to 1000°C at a heating rate of 10°C/min. As a representative case, the TG/DTG curve of **C1** is depicted in Figure 5. The TGA/DTG data of complexes are summarized in Table 2.

The thermal decomposition of **C1** occurs in three stages. The first stage proceeded with two degradation steps with the weight loss of 6% (calcd 7.18%) in the temperature range of 148–222°C with DTG peaks observed at 148 and 222°C. This weight loss is due to the simultaneous loss of coordinated water molecule and chlorine atom. The second stage continued with one degradation step with the weight loss of 40% (calcd 41.07%) in the temperature range of 230–490°C with DTG peak observed at 347°C. This weight loss is due to the loss of $C_{19}H_{15}NO_3$ fragment. The third stage occurred at the temperature range of 490–800°C with the weight loss of 42% (calcd 43.37%) due to the loss of $C_{20}H_{26}N_4$ fragment with DTG peak observed at 660°C. The overall weight loss observed in **C1** was found to be 88% (calcd 91.62%). The metallic Cu left as the residue has the observed weight of 10% against the calculated value of 11%.

Complex **C2** underwent degradation in three stages. The first stage occurred at the temperature range of 100–220°C with a weight loss of 6.50% (calcd 7.24%). The DTG peaks were observed at 142 and 220°C. This weight loss is due to the simultaneous loss of one coordinated water molecule and chlorine atom. The complex underwent further degradation at the temperature range of 220–480°C, with the loss of 40.50% (calcd 41.33) and the DTG peak was observed at 315°C. This weight loss is due to the loss of $C_{19}H_{15}NO_3$fragment. The third stage of degradation occurred at the temperature range of 480–880°C, with the loss of 42.40% (calcd 43.64%) and the DTG peak was observed at 674°C. This weight loss is due to the loss of $C_{20}H_{26}N_4$ fragment. The overall weight loss was found to be

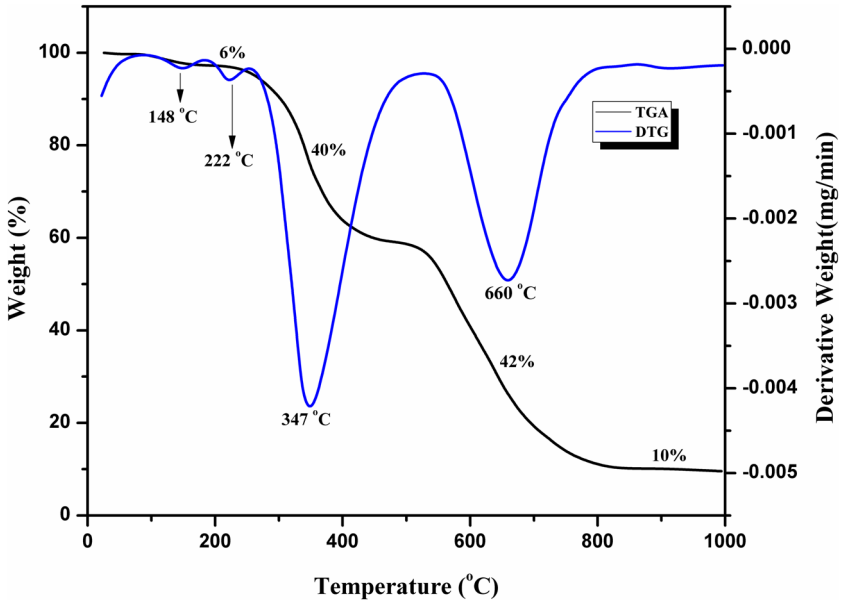

FIGURE 5 Thermogravimetric analysis (TGA) and DTG curves of complex **C1**

89.40% (calcd 92.21%). The metallic Co left as a residue has the observed weight of 10.60% against the calculated value of 7.79%.

The thermogram of **C3** showed degradation in three stages. The first degradation occurred at the temperature range of 100–240°C with the loss of 6% (calcd 7.22%), and the DTG peaks were observed at 130 and 229°C. This weight loss is due to the loss of one coordinated water molecule and chlorine atom. The second stage of degradation occurred at the temperature range of 240–500°C with the loss of 40% (calcd 41.37%) with the DTG peak observed at 376°C. This weight loss is due to the loss of $C_{19}H_{15}NO_3$ fragment. The third stage of degradation occurred at the temperature range of 500–920°C with the loss of 43% (calcd 43.8%), and the DTG peak was observed at 754°C. This weight loss is due to the loss of $C_{20}H_{26}N_4$ fragment. The total weight loss was found to be 89% (calcd 92.39%). The metallic Ni left as a residue has the observed weight of 11% against the calculated value of 7.61%.

The thermogram of **C4** showed the first stage of degradation due to the simultaneous loss of one coordinated water molecule and one chlorine atom at the temperature range of 100–250°C with the loss of 6% (calcd 7.18%). The DTG peaks were observed at 120 and 220°C. The complex underwent further degradation due to the loss of $C_{19}H_{15}NO_3$ fragment at the temperature range of 250–540°C with the loss of 41% (calcd 41.03%). The DTG peak was observed at 287°C. The third stage of degradation occurred due to the loss of $C_{20}H_{26}N_4$ fragment at the temperature range of 540–790°C with the loss of 43% (calcd 43.35%). The DTG peak was observed at 710°C. The overall weight loss was found to be 90% (calcd 91.56%). The metallic Zn left as a residue has the observed weight of 10% against the calculated value of 8.44%.

4.7 | Minimum inhibitory concentration and minimum fungicidal concentrations

The antifungal activity of all the newly synthesized ligands and their complexes was evaluated by determining their MIC and MFC values against 11 different *C. albicans* strains, including one laboratory standard strain, seven FLC-susceptible clinical strains and three FLC-resistant clinical strains. All the MIC results are summarized in Table 3. Evaluation of MIC depicts that among the two ligands and their four complexes, **C3** showed the highest inhibitory activity, while both ligands (**L1** and **L2**) showed the least inhibitory activity against all the tested strains. Based on the MIC values, the order of potency of the test compounds was **C3** > **C2** > **C1** > **C4** > **L1** ≥ **L2**. The median MIC values for **C3**, **C2**, **C1**, **C4**, **L1** and **L2** are 0.10, 0.40, 6.25, 12.5, 100 and 100, respectively. FLC was also tested, and the isolates with MIC values < 8 μg/mL for FLC were considered FLC-susceptible while the isolates with MIC ≥ 8 μg/mL were categorized as FLC-resistant, following the CLSI Interpretive Guidelines for *In vitro* Susceptibility Testing of *Candida* species.[31] Furthermore, all the test compounds were prepared to different concentrations using 1% DMSO, and therefore DMSO was used as negative vehicle control and was observed to have no inhibitory activity against any of the tested isolates. The MIC data revealed that the structural changes from ligand to its metal complexes produced the marked enhancement in their potency as antifungal agents.

The MFC is the lowest concentration of the test compounds that causes death of cells that can be observed on clear agar plates. Table 3 summarizes the MFC values of all the test compounds against 11 tested *C. albicans* isolates. Except two ligands (**L1**, **L2**), all the derivatives showed MFC values, depicting the fungicidal activity of newly synthesized compounds. The MFC values are generally two–fourfold higher than MIC values.

4.8 | Sterol quantitation

The antifungal effect of the tested compounds was rapid and lethal. The rapid irreversible action of the active complexes suggests that there may be a cellular target accessible to the compound externally. Therefore, we studied the effect of these active complexes on sterol biosynthesis. Figure 6 and Table S2 summarize the effect of these compounds on ergosterol biosynthesis in FLC-susceptible and -resistant *C. albicans* isolates at MIC and ½ MIC values of all the newly synthesized compounds. Sterol patterns were altered in a similar manner in FLC-susceptible and -resistant isolates when cells were treated with subinhibitory concentrations of the test compounds. These compounds completely blocked ergosterol synthesis at MIC values (Figure 6). As shown in Table S2, the decrease in total cellular ergosterol content for susceptible isolates ranged from 21% to 57% for cells grown in ½ MIC values to 62% to 93% for cells grown with MIC values of the test compounds. Similarly, for resistant isolates, the decrease in total cellular ergosterol content ranged from 28% to 63% when treated with ½ MIC, and 71% to 97% when treated with MIC values of the test compounds, respectively. As expected, the decrease in total cellular ergosterol content of susceptible cells treated with FLC was measured to be 96%. In contrast to this, resistant isolates only showed decline in ergosterol content by 37%.

Ergosterol and its biosynthesis pathway is an established drug target for different classes of antifungal drugs including that of azoles and polyenes. There are several studies reporting that the manipulation of this drug target is responsible for drug resistance in different fungal species including *C. albicans*. Our results clearly indicate that the resistant isolates used in this study are resistant due to the overexpression of ergosterol. The survival of these cells at ½ MIC values of the test compounds, where more than 50% ergosterol biosynthesis was inhibited, indicate that these *C. albicans* isolates belong to ergosterol-tolerant class. Due to the structural variability of these compounds, it is possible that they interact with different enzymes of the ergosterol pathway and thereby inhibit its biosynthesis. However, further in-depth studies are required to elucidate the actual binding of these compounds with the specific enzymes.

4.9 | Effect on membrane integrity

The effect of active compounds (**C1–C4**) on disruption of membrane integrity in *C. albicans* was studied using flow

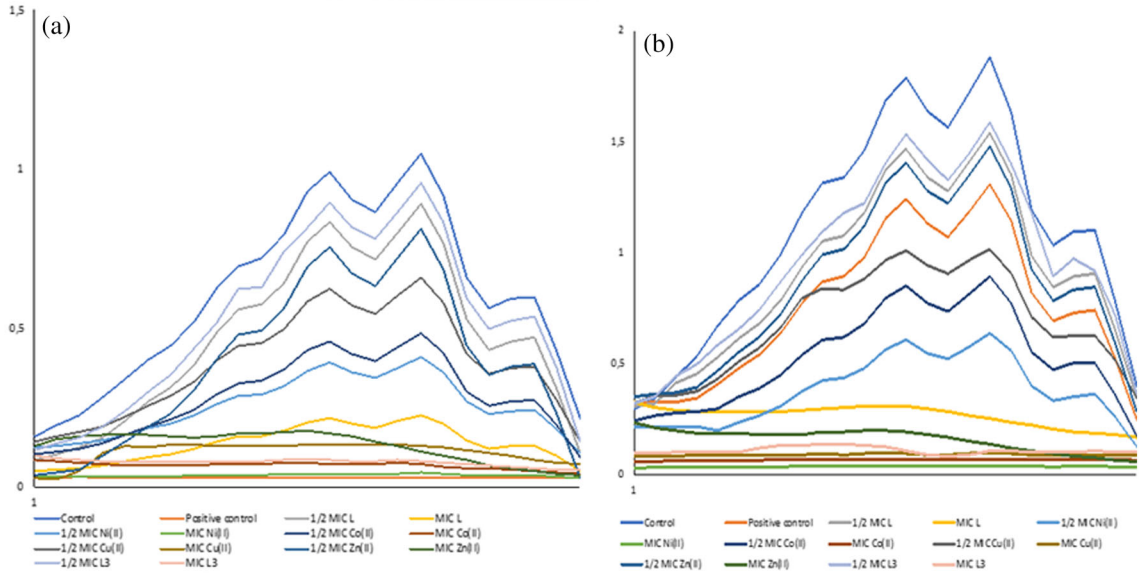

FIGURE 6 UV spectrophotometric sterol profiles of representative fluconazole(FLC)-susceptible (a) and FLC-resistant (b) *Candida albicans* isolates. Isolates were grown for 16 hr in Sabouraud Dextrose (SD) broth containing ½ minimum inhibitory concentration (MIC) and MIC values of two ligands and four derivatives. Sterols were extracted from cells, and spectral profiles in the range 240–300 nm were determined. Control represents untreated cells, while positive control represents cells treated with 2 μg/mL of FLC

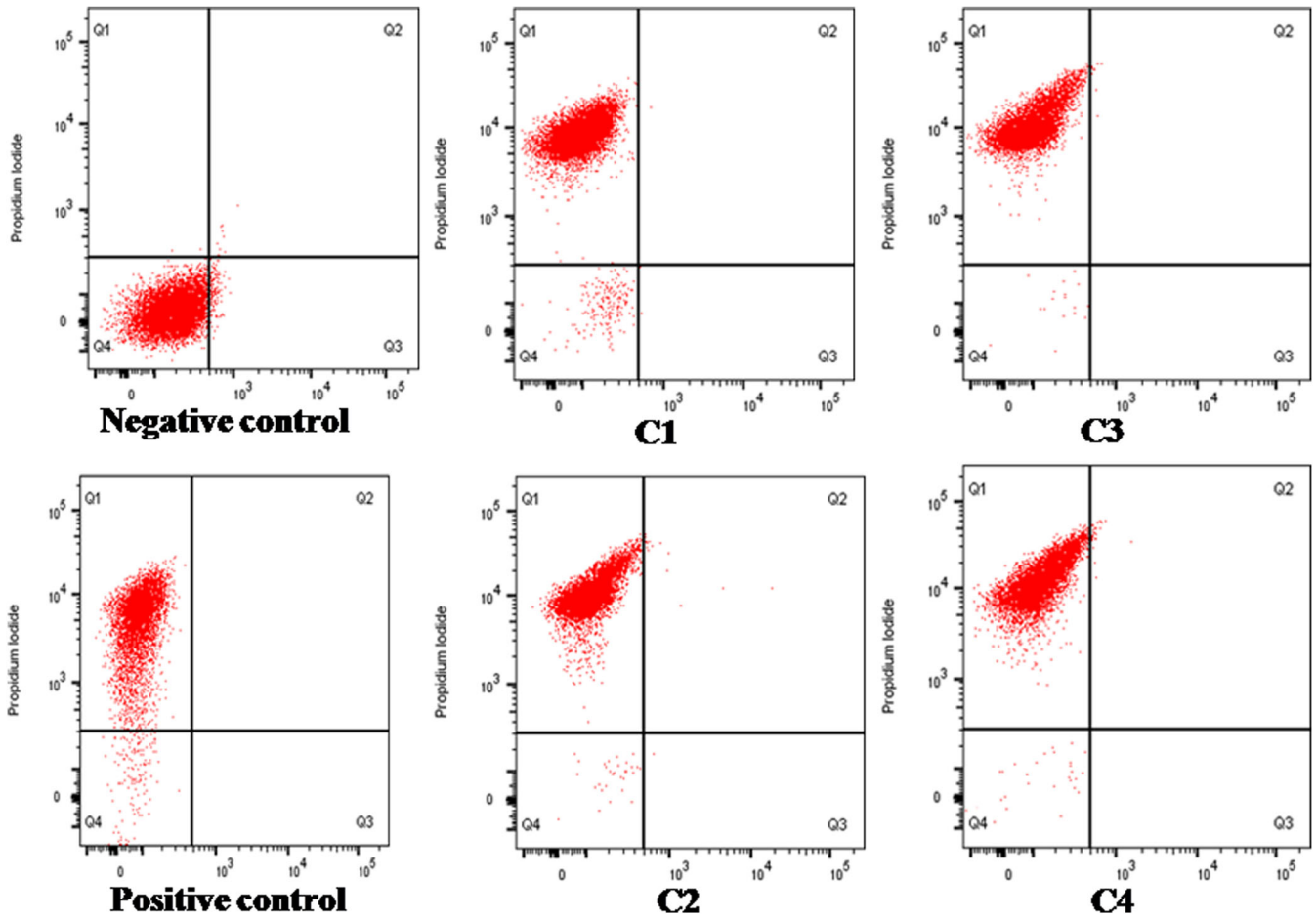

FIGURE 7 Sequence of density plots showing *Candida albicans* SC5314 cells analyzed by flow cytometry for the samples treated with minimum fungicidal concentrations (MFCs) of compounds **C1**, **C2**, **C3** and **C4**. Negative and positive controls are untreated and 2 μg/ml amphotericin B-treated cells, respectively. Density plots show relative fluorescence intensities of *Candida* cells marked with propidium iodide (PI) on the *y*-axis. The lower left quadrant (Q4) marked the morphologically intact live cells observed with higher relative fluorescence intensity, while the upper left grid (Q1) marked dead cells

cytometer. PI is the most commonly used fluorescent dye to study the effect of drugs on cell membranes. Live cells with integrated membranes will not allow PI to internalize the cells; however, dead cells with disintegrated membranes internalize PI, resulting in an increase in red fluorescence.[24] The PI penetration in *C. albicans* cells treated with MFC values of test compounds along with negative and positive controls are summarized in Figure 7. All the four tested compounds along with amphotericin B at MFC values showed >90% PI internalization, indicating that these compounds have a potential to disintegrate cell membranes at the higher concentrations similarly to that of amphotericin B.

The membrane damage in collaboration with the inhibition of ergosterol biosynthesis by these derivatives can contribute to membrane malfunctioning resulting in membrane depolarization, intracellular content leakage, disturbance in membrane permeability and ultimately cell death. The results in this study are in congruent with the previous findings where derivatives from natural products have been reported to disrupt fungal membrane integrity causing cell death.[24,32]

5 | CONCLUSIONS

In this study, some heteroleptic complexes derived from two Schiff base ligands, obtained from biologically important scaffolds were synthesized in a quest to find better antifungal therapeutic agents. With the help of spectral and other physical measurements, an octahedral geometry was assigned to the complexes **C2**, **C3** and **C4**, while a distorted octahedral geometry was assigned to the complex **C1**. The antifungal activity evaluation against susceptible and resistant *C. albicans* revealed that both the ligands have moderate activity, while derivative complexes have strong antifungal activity. Insight mechanisms revealed that these complexes disrupt cell membranes and also deplete ergosterol content. To conclude, this work suggests that these compounds could

be promising antifungal drugs, and also advocates the determination of optimal concentrations for clinical applications for the treatment and prevention of candidiasis. The excellence of these compounds demands more insight studies into all other possible mechanisms.

ACKNOWLEDGEMENTS

The author OAD is thankful to University Grants Commission (UGC), Government of India for financial assistance through Central University Ph.D. Students Fellowship. AA acknowledges financial support from University Research Committee Grant for 2019 - Friedel Sellschop Award (Grant No: AZMD019). The funders had no role in study design, data collection and analysis, decision to publish, or preparation of the manuscript.

CONFLICT OF INTEREST

The authors declare that they have no competing interests.

ORCID

Shabir Ahmad Lone https://orcid.org/0000-0003-1850-9625
Mohmmad Younus Wani https://orcid.org/0000-0002-1838-1337
Aijaz Ahmad https://orcid.org/0000-0003-2845-0727

REFERENCES

[1] M. E. Rodrigues, S. Silva, J. Azeredo, M. Henriques, *Crit. Rev. Microbiol.* **2016**, *42*, 594.
[2] F. L. Van De Veerdonk, M. G. Netea, L. A. Joosten, J. W. M. Van De Meer, B. J. Kullberg, *FEMS Microbiol. Rev.* **2010**, *34*, 1063.
[3] D. W. Denning, *Philos. Trans. R. Soc. B Biol. Sci.* **2016**, *371*. 20 150 468.
[4] M. A. Pfaller, D. J. Diekema, D. L. Gibbs, V. A. Newell, J. F. Meis, I. M. Gould, W. Fu, A. L. Colombo, E. Rodriguez-Noriega, *J. Clin. Microbiol.* **2007**, *45*, 1735.
[5] N. M. Revie, K. R. Iyer, N. Robbins, L. E. Cowen, *Curr. Opin. Microbiol.* **2018**, *45*, 70.
[6] N. Robbins, T. Caplan, L. E. Cowen, *Annu. Rev. Microbiol.* **2017**, *71*, 753.
[7] S. Wu, Y. Wang, N. Liu, G. Dong, C. Sheng, *J. Med. Chem.* **2017**, *60*, 2193.
[8] K. D. Mjos, C. Orvig, *Chem. Rev.* **2014**, *114*, 4540.
[9] Y. C. Ong, S. Roy, P. C. Andrews, G. Gasser, *Chem. Rev.* **2019**, *119*, 730.
[10] M. Zaki, F. Arjmand, S. Tabassum, *Inorgan. Chim. Acta* **2016**, *444*, 1.
[11] K. J. Kilpin, P. J. Dyson, *Chem. Sci.* **2013**, *4*, 1410.
[12] K. L. Haas, K. J. Franz, *Chem. Rev.* **2009**, *109*, 4921.
[13] L. J. Boerner, J. M. Zaleski, *Curr. Opin. Chem. Biol.* **2005**, *9*, 135.
[14] M. Shebl, *Spectrochim. Acta Part A Mol. Biomol. Spectrosc.* **2014**, *117*, 127.
[15] X. Liu, C. Manzur, N. Novoa, S. Celedón, D. Carrillo, J.-R. Hamon, *Coord. Chem. Rev.* **2018**, *357*, 144.
[16] K. Mancha Madha, P. Gurumoorthy, S. Arul Antony, N. Ramalakshmi, *J. Mol. Struct.* **2017**, *1143*, 478.
[17] M. A. Malik, O. A. Dar, P. Gull, M. Y. Wani, A. A. Hashmi, *Medchemcomm.* **2018**, *9*, 409.
[18] A. M. Asiri, S. A. Khan, H. M. Marwani, K. Sharma, *J. Photochem. Photobiol. B Biol.* **2013**, *120*, 82.
[19] M. Y. Nassar, H. M. Aly, M. E. Moustafa, E. A. Abdelrahman, *J. Inorg. Organomet. Polym. Mater.* **2017**, *27*, 1220.
[20] M. Y. Nassar, H. M. Aly, E. A. Abdelrahman, M. E. Moustafa, *J. Mol. Struct.* **2017**, *1143*, 462.
[21] W. H. Mahmoud, G. G. Mohamed, O. Y. El-Sayed, *Appl. Organomet. Chem.* **2018**, *32*, e4051.
[22] CLSI-Clinical and Laboratory Standards Institute Standards, Wayne, PA, USA, **2008**, 40.
[23] A. Ahmad, M. Y. Wani, A. Khan, N. Manzoor, J. Molepo, *PLoS ONE* **2015**, *10*, e0145053.
[24] A. Khan, A. Ahmad, F. Akhtar, S. Yousuf, I. Xess, L. A. Khan, N. Manzoor, *Res. Microbiol.* **2010**, *161*, 816.
[25] G. Ahumada, T. Roisnel, S. Kahlal, D. Carrillo, R. Córdova, J.-Y. Saillard, J.-R. Hamon, C. Manzur, *Inorgan. Chim. Acta* **2018**, *470*, 221.
[26] J. Devi, N. Batra, *Spectrochim. Acta Part A Mol. Biomol. Spectrosc.* **2015**, *135*, 710.
[27] M. M. Abo-Aly, A. M. Salem, M. A. Sayed, A. A. Abdel Aziz, *Spectrochim. Acta Part A Mol. Biomol. Spectrosc.* **2015**, *136*, 993.
[28] P. Gull, O. A. Dar, M. A. Malik, A. A. Hashmi, *Microb. Pathog.* **2016**, *100*, 237.
[29] J. H. Pandya, R. N. Jadeja, K. J. Ganatra, *J. Saudi Chem. Soc.* **2014**, *18*, 190.
[30] M. A. Estermann, W. I. F. David in: W. I. F. David, K. Shankland, B. Mccusker, Ch. Baerlocher(Eds.), Structure determination from powder diffraction data (SDPD), Oxford Science Publications, New York, **2002**.
[31] CLSI-Clinical and Laboratory Standards Institute, 2012 (Document M27-S4).
[32] D. G. Yun, D. G. Lee, *Biochim. Biophys. Acta, Biomembr.* **2017**, *1859*, 467.

SUPPORTING INFORMATION

Additional supporting information may be found online in the Supporting Information section at the end of the article.

How to cite this article: Dar OA, Lone SA, Malik MA, et al. Heteroleptic transition metal complexes of Schiff-base-derived ligands exert their antifungal activity by disrupting membrane integrity. *Appl Organometal Chem*. 2019;e5128. https://doi.org/10.1002/aoc.5128